Response of Marine Boundary Layer Cloud Properties to Aerosol Perturbations Associated with Meteorological Conditions from the 19-Month AMF-Azores Campaign

JIANJUN LIU

Earth System Science Interdisciplinary Center, University of Maryland, College Park, College Park, Maryland

ZHANQING LI

Earth System Science Interdisciplinary Center, University of Maryland, College Park, College Park, Maryland, and State Laboratory of Earth Surface Process and Resource Ecology, College of Global Change and Earth System Science, Beijing Normal University, Beijing, China

MAUREEN CRIBB

Earth System Science Interdisciplinary Center, University of Maryland, College Park, College Park, Maryland

(Manuscript received 8 December 2015, in final form 15 July 2016)

ABSTRACT

This study investigates the response of marine boundary layer (MBL) cloud properties to aerosol loading by accounting for the contributions of large-scale dynamic and thermodynamic conditions and quantifies the first indirect effect (FIE). It makes use of 19-month measurements of aerosols, clouds, and meteorology acquired during the Atmospheric Radiation Measurement Mobile Facility field campaign over the Azores. Cloud droplet number concentrations N_c and cloud optical depth (COD) significantly increased with increasing aerosol number concentration N_a. Cloud droplet effective radius (DER) significantly decreased with increasing N_a. The correlations between cloud microphysical properties [N_c, liquid water path (LWP), and DER] and N_a were stronger under more stable conditions. The correlations between N_c, LWP, DER, and N_a were stronger under ascending-motion conditions, while the correlation between COD and N_a was stronger under descending-motion conditions. The magnitude and corresponding uncertainty of the FIE $\{=[-\partial \ln(\mathrm{DER})/\partial \ln(N_a)]$ at constant LWP$\}$ ranged from 0.060 ± 0.022 to 0.101 ± 0.006 depending on the different LWP values. Under more stable conditions, cloud-base heights were generally lower than those under less stable conditions. This enabled a more effective interaction with aerosols, resulting in a larger value for the FIE. However, the dependence of the response of cloud properties to aerosol perturbations on stability varied according to whether ground- or satellite-based DER retrievals were used. The magnitude of the FIE had a larger variation with changing LWP under ascending-motion conditions and tended to be higher under ascending-motion conditions for clouds with low LWP and under descending-motion conditions for clouds with high LWP. A contrasting dependence of FIE on atmospheric stability estimated from the surface and satellite cloud properties retrievals reported in this study underscores the importance of assessing all-level properties of clouds in aerosol–cloud interaction studies.

1. Introduction

One of the largest uncertainties in climate change studies arises from the poor understanding of aerosol indirect effects (AIE), which are now referred to as aerosol–cloud interactions in the latest Intergovernmental Panel on Climate Change (IPCC) report (IPCC 2013). The scattering and absorption of solar radiation by aerosol particles is called the aerosol direct effect on Earth's radiation field. The AIE involves more cloud microphysical processes. The first indirect effect (FIE) is called the Twomey effect. Assuming that the cloud liquid water path (LWP) is constant, the number of cloud condensation nuclei (CCN) will increase as the number of atmospheric aerosol particles increases, which results in more small cloud

Corresponding author address: Zhanqing Li, ESPRE, GCESS, Beijing Normal University, 19 Xinjiekouwai Street, Haidian District, Beijing 100875, China.
E-mail: zhanqingli@msn.com

DOI: 10.1175/JAS-D-15-0364.1

© 2016 American Meteorological Society

droplets and more reflection of energy to space (Twomey 1977). This has a cooling effect on Earth's surface. The presence of more small cloud droplets will reduce the chances of precipitation forming, resulting in a longer-living cloud (the second indirect effect; Albrecht 1989). AIE are the dominant contributors to the overall aerosol radiative forcing in most climate models yet are poorly constrained and can vary by a factor of 5 across different models (Quaas et al. 2009; Wood et al. 2015).

Marine boundary layer (MBL) clouds are common over the subtropical and midlatitude oceans and are particularly susceptible to perturbations in aerosols (Wood et al. 2015). These clouds strongly influence regional and global climate systems. Interactions between MBL clouds and aerosols are important components of the climate system and are also one of the largest sources of uncertainty in predicting any potential future climate change (Bony and Dufresne 2005; Dong et al. 2014a). Microphysical, structural, and dynamic properties of MBL clouds are all sensitive to aerosol loading, but their responses are not uniform (Dong et al. 2014a,b; Logan et al. 2014; Dong et al. 2015). The question of what processes control the diversity in the sensitivity of warm clouds to aerosol perturbations is one of the important science questions that has arisen in studies of cloud–aerosol–precipitation interactions. It is a major source of uncertainty that thwarts the accurate prediction of future climate change (Wood 2009).

The observed responses of warm low-level cloud properties to aerosols in a marine environment have been studied in recent years based on multiple observations, such as those from satellite-based remote sensing (Nakajima et al. 2001; Menon et al. 2008; Su et al. 2010; Wang et al. 2014; Dong et al. 2014a, 2015), from surface-based remote sensing (Feingold et al. 2001, 2003; McComiskey et al. 2009; Pandithurai et al. 2009), and from aircraft (Zheng et al. 2010; Painemal and Zuidema 2013; Twohy et al. 2013). However, satellite remote sensing suffers from several inherent retrieval problems (Li et al. 2009; Xi et al. 2014). There is also the limitation that cloud and aerosol properties cannot be obtained simultaneously over the same location. Recent studies have revealed that the aerosol optical depth (AOD) retrieved in the presence of nearby clouds can be significantly enhanced (Jeong and Li 2010; Várnai and Marshak 2014), which can lead to spurious correlations between aerosols and cloud properties (Costantino and Bréon 2013). These limitations can be ameliorated, or overcome, by using ground and in situ observations, which have already been used to investigate the influence of aerosols on cloud microphysical properties (Feingold et al. 2001, 2003; McComiskey et al. 2009; Twohy et al. 2013). An advantage of this approach is that the effect of aerosols on clouds can be examined in a single column of air at the scale of cloud droplet formation and at high temporal and spatial resolutions. Most surface- and aircraft-based analyses are done on a case-by-case basis. MBL cloud macro- and microphysical properties are likely correlated with variations in large-scale meteorological forcing [e.g., lower-tropospheric stability (LTS; Wood and Bretherton 2006)] and with aerosol properties. This suggests that a long data record is needed to disentangle the meteorological impact from aerosol effects on clouds (Teller and Levin 2006; Wood 2009; Koren et al. 2010).

With the goal of better understanding the seasonal and diurnal variations in MBL cloud properties and their response to aerosol perturbations, the Atmospheric Radiation Measurement (ARM) Mobile Facility (AMF) was deployed to a site on the northern coast of Graciosa Island in the Azores (39.09°N, 28.03°W) from May 2009 to December 2010 (Wood et al. 2015). The site is located in the northeast Atlantic Ocean, where MBL clouds are omnipresent throughout the year because of the presence of semipermanent high pressure systems (Dong et al. 2014a; Wood et al. 2015). The primary goal of this study is to investigate the response of MBL nonprecipitating cloud properties to changes in aerosol loading and to determine how meteorological parameters affect the diversity in the sensitivity of MBL nonprecipitating clouds to aerosol perturbations and the magnitude of the aerosol FIE.

A brief description of measurements and methods used in the analyses is given in section 2. The statistical properties of aerosols, clouds, and meteorological properties, the response of cloud properties to aerosol perturbations, and the influence of meteorological conditions on these responses are given in section 3. The quantified FIE and the dependence of the magnitude of FIE on meteorological parameters are also presented in section 3. Conclusions are given in section 4.

2. Data and methods

Aerosol number concentrations N_a were selected to represent aerosol loading in this study, because N_a is a better proxy of CCN concentration than are aerosol optical properties (Liu et al. 2011; Li et al. 2011; Liu and Li 2014). The ARM Aerosol Observation System (AOS) is the primary platform used for collecting aerosol concentration data, aerosol scattering and absorption properties, and aerosol composition properties at the surface (Jefferson 2011). The TSI model 3010 particle counter is a compact and rugged instrument installed in the AOS trailer that measured the N_a of particles with diameters ranging from 10 nm to 3 μm in 1-min intervals during the field campaign in the Azores.

The macro- and microphysical properties of MBL clouds, defined in this study as clouds with cloud-top

heights (CTH) less than 3 km (Dong et al. 2014a), are extracted from the ARM principal investigator product, which combines retrievals from the W-band ARM cloud radar (WACR), the Vaisala ceilometer, the micropulse lidar (MPL), and the microwave radiometer (MWR). Parameters include the cloud-base height (CBH), CTH, cloud droplet number concentrations N_c, cloud LWP, cloud optical depth (COD), and cloud droplet effective radius (DER) averaged over 5-min intervals. The products have been used to investigate MBL cloud properties (Dong et al. 2014a,b, 2015) and to validate MBL cloud properties retrieved from the NASA Clouds and the Earth's Radiant Energy System project using Moderate Resolution Imaging Spectroradiometer (MODIS) data (Xi et al. 2014). Details about each parameter can be found at the ARM website (http://www.arm.gov/data/pi/88).

Cloud-base height is derived from a composite of ceilometer, MPL, and WACR data (Clothiaux et al. 2000; Wang and Sassen 2001; Mather and Voyles 2013), while the CTH is obtained from the combination of WACR cloud reflectivity profiles and MPL measurements (Clothiaux et al. 2000; Wang and Sassen 2001). Cloud LWP is retrieved from MWR-measured brightness temperatures at 23.8 and 31.4 GHz using the statistical approach developed by Liljegren et al. (2001). Typical uncertainties in the retrieved LWP are $\sim 20\,\mathrm{g\,m^{-2}}$ for LWP $< 200\,\mathrm{g\,m^{-2}}$ and 10% for LWP $> 200\,\mathrm{g\,m^{-2}}$ (Dong et al. 2000; Liljegren et al. 2001). The layer-mean DER, N_c, and COD are derived from the parameterization method developed by Dong et al. (1998, 2014a). The DER is parameterized as

$$\mathrm{DER} = -2.07 + 2.49\mathrm{LWP} + 10.25\gamma - 0.25\mu_0 + 20.28\mathrm{LWP}(\gamma) - 3.14\mathrm{LWP}(\mu_0),$$

where γ is the solar transmission and μ_0 is the cosine of the solar zenith angle. The N_c is calculated as

$$N_c = \frac{3\mathrm{LWP}}{4\pi\rho_w r_e^3 \Delta z}\exp(3\sigma_x^2),$$

where r_e is the cloud droplet effective radius, ρ_w is the density of water, Δz is the layer thickness, and σ_x is the logarithmic width set at a constant value of 0.38. The uncertainty in the estimation of N_c based on this parameterization is ~20%–30%. The COD is calculated as

$$\mathrm{COD} = \frac{3\mathrm{LWP}}{2\rho_w r_e}.$$

Retrieved and parameterized low-cloud microphysical properties have been validated by aircraft in situ measurements at the Azores, and their uncertainties (~10% for DER and COD retrievals) have been discussed in studies by Dong et al. (1998, 2014a,b, 2015) and Dong and Mace (2003). Dong et al. (1997, 1998, 2000) provide more detailed descriptions about the retrieval methods and parameterizations.

Cloud macro- and microphysical properties are significantly influenced by atmospheric dynamic and thermodynamic conditions. The vertical velocity ω at 700 hPa has been extensively used to constrain the dynamic condition (Bony et al. 2004; Medeiros and Stevens 2011; Su et al. 2010). LTS is typically used to constrain the thermodynamic condition (Matsui et al. 2004; Lebsock et al. 2008; Wang et al. 2014; Dong et al. 2015) and is calculated as the difference between the potential temperature of the free troposphere (700 hPa) and the surface. The ω and LTS are obtained from the European Centre for Medium-Range Weather Forecasts (ECMWF) model runs for ARM analysis provided by the ECMWF (ECMWF 1994). Output from model runs are generated hourly for a 0.56° × 0.56° box centered on the site and include zonal and meridional wind components, temperature, relative humidity, and vertical velocity at 91 pressure levels from the surface to 10 hPa.

In this study, clouds with LWP $< 20\,\mathrm{g\,m^{-2}}$ (when retrieval errors are large) or LWP $> 700\,\mathrm{g\,m^{-2}}$ (when precipitation contamination likely occurs) (Dong et al. 2008) were excluded. After matching N_a and cloud properties according to the observation time, they were then matched with hourly ECMWF simulation output parameters.

3. Results

a. *Aerosol and cloud properties and meteorological conditions*

Before investigating the relationship between aerosol and MBL cloud properties, the probability distribution function (PDF) and cumulative distribution function (CDF) of N_a, cloud macro- and microphysical properties, and atmospheric dynamic and thermodynamic properties during the period of study are first examined (Fig. 1). Numbers in each panel are mean values with their standard deviations. This figure gives an overall view of the range of cloud, aerosol, and meteorological conditions observed during the 19-month period. The mean and standard deviation of N_a are 509 and $323\,\mathrm{cm^{-3}}$, respectively, with a mode value of 300–400 $\mathrm{cm^{-3}}$. Roughly 80% of the N_a values are less than $700\,\mathrm{cm^{-3}}$.

The CBH distribution (Fig. 1b) shows that almost all cloud bases are lower than 2 km and that nearly 60% of CBHs are less than 1 km with a peak between 0.6 and 0.8 km. Most cloud tops are located between 1 and 2 km (Fig. 1c), accounting for ~60% of total samples. These are typical values for MBL clouds. The mean (plus or minus

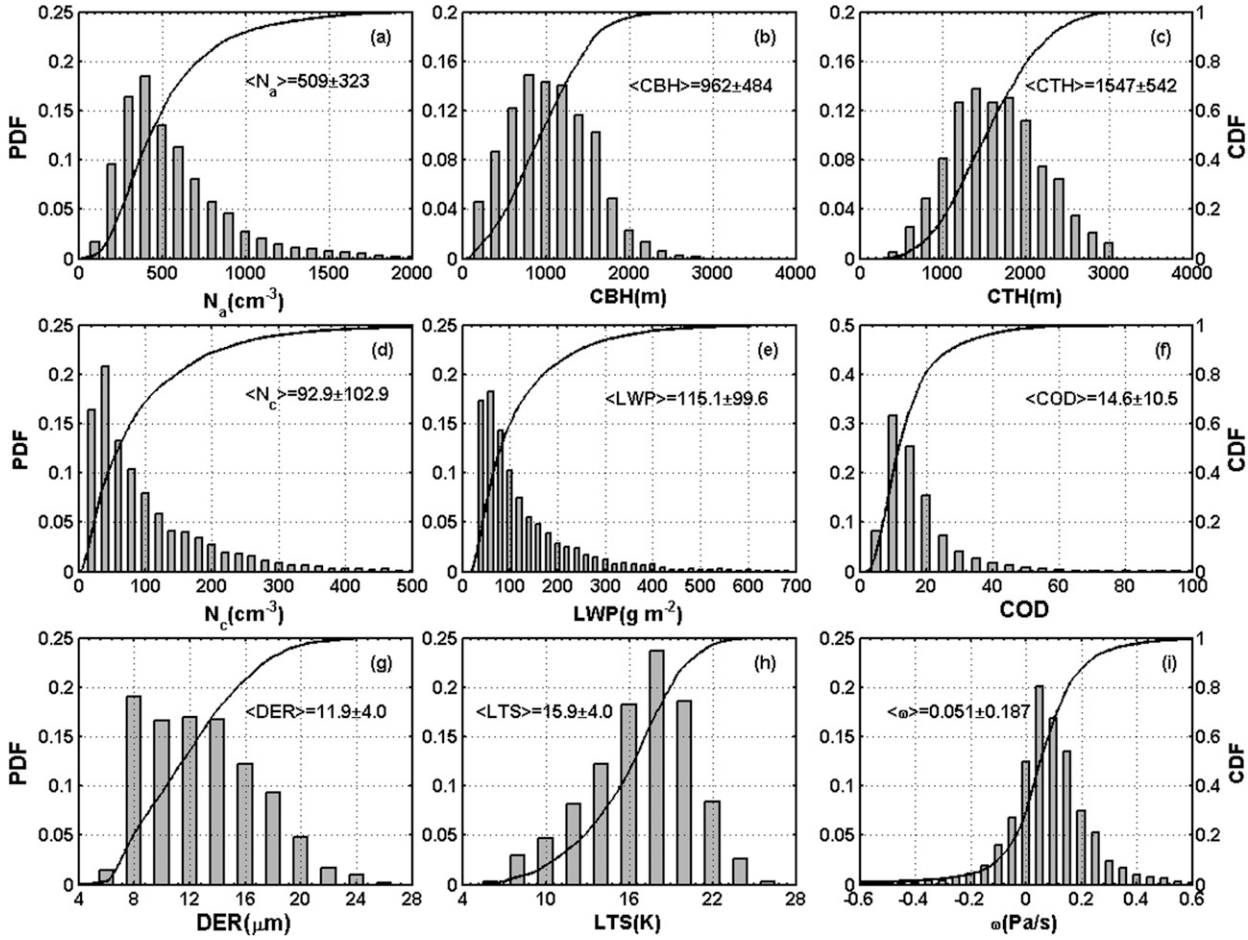

FIG. 1. PDFs (bars) and CDFs (curves) of (a) N_a, (b) CBH, (c) CTH, (d) N_c, (e) LWP, (f) COD, (g) DER, (h) LTS, and (i) ω during the study period. Numbers in each panel are the mean value plus or minus one std dev.

one standard deviation) CBH and CTH are 0.96 ± 0.48 and 1.55 ± 0.54 km, respectively. Clouds with relatively low CBH are in more contact with aerosols because the majority of aerosols are confined to the boundary layer (Liu et al. 2012; Huang et al. 2013). The mean value of N_c is 92.9 cm^{-3} with a standard deviation of 102.9 cm^{-3}. Nearly 80% of N_c values are less than 140 cm^{-3}, and more than 20% of all values are between 20 and 40 cm^{-3}. More than 80% of LWP values are less than 180 g m^{-2}, and ~60% of all values are less than 100 g m^{-2}. The mean value of LWP during the period of study is 115.1 ± 99.6 g m^{-2} with peaks in the range of 40–60 g m^{-2}. Figure 1f shows that the mean COD is 14.6 ± 10.5. Clouds with COD less than 20 account for 80% of all samples, and the maximum distribution falls in the range of 5–10. The mean value of DER is 11.9 ± 4.0 μm (Fig. 1g), which is consistent with the values reported by Dong et al. (1997, 2014a) and Miles et al. (2000). This value represents a typical MBL cloud DER (Dong et al. 1997, 2014a). About 65% of all DER values range from 6 to 14 μm.

The distributions of LTS and ω are given in Figs. 1h and 1i, respectively. More than 70% of LTS values are greater than 14 K, and nearly 50% of all values fall in the range of 14–20 K with a mean value of 15.9 ± 3.7 K. The PDF of ω is a near-normal distribution with a peak at 0–0.05 Pa s^{-1}. About 70% of all values are greater than 0, which indicates that descending motions dominate most clouds. The large fraction of ω with small absolute values shows that most clouds have weak ascending and descending motions.

b. *Variations in cloud properties with aerosol loading*

Figure 2 shows variations in N_c, LWP, DER, and COD with increasing N_a. The error bars represent the standard deviation of the mean value (i.e., $\sigma/\sqrt{n-2}$), where σ and n are the standard deviation of the cloud property measurements and the number of independent

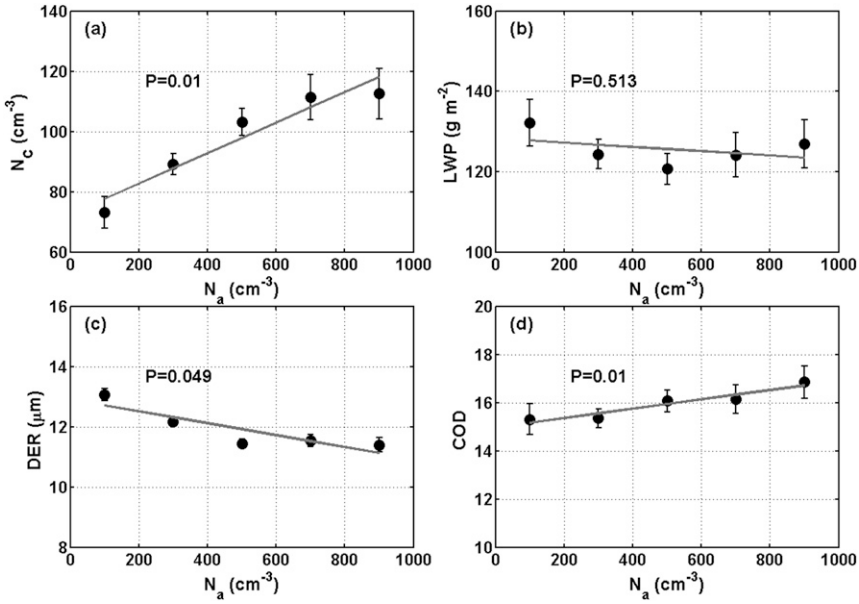

FIG. 2. (a) N_c, (b) LWP, (c) DER, and (d) COD as a function of N_a. The statistical probability (P value) is shown.

data points, respectively, within a bin, determined using the method described by Leith (1973). The N_c increases significantly with increasing N_a. This is expected because more aerosols will generate more CCN and therefore more N_c. Figure 2b shows that LWP decreases slightly with increasing N_a, but not significantly so. Current studies about the response of LWP to increases in aerosol loading are diverse, showing a positive correlation in some studies (Quaas et al. 2009; Wang et al. 2013) and a negative correlation in others (Twohy et al. 2005; Lee et al. 2009). Wang et al. (2013) found that LWP increased in marine stratocumulus clouds under high aerosol loading conditions as a result of suppressed drizzle production. The negative correlation in this study may be because the inhibited cloud droplet sedimentation due to the reduced cloud droplet size likely enhances evaporation and entrainment at the cloud top, resulting in a reduction in LWP (Kaufman et al. 2005; Bretherton et al. 2007; Hill and Feingold 2009). This is supported by the result that cloud thickness increases with increasing N_a (figure not shown), because cloud thickness should increase as a result of increased entrainment. Figure 2b also strongly suggests that the assumption of a constant LWP is valid and reasonable for AIE studies. Figures 2c and 2d show that, as aerosol loading increases, DER significantly decreases and COD significantly increases. Assuming no associated change in meteorological variables, which is investigated in another section, this finding implies that aerosols enhance the attenuation property of clouds by increasing N_c and by inhibiting the growth of cloud droplets (Twomey 1977).

The PDFs and CDFs of each cloud property under high and low aerosol loading conditions are presented in Fig. 3. The numbers in each panel are the differences in each cloud property between low and high aerosol loading conditions. The difference is defined as $\{[(M_{c_h} - M_{c_l})/M_{c_l}] \times 100\%\}$, where M_{c_h} is the mean value of the cloud property under high aerosol loading conditions and M_{c_l} is the mean value of the cloud property under low aerosol loading conditions. Measurements of N_a less than the overall median value of N_a are considered to be measurements made under low aerosol loading conditions, and measurements of N_a greater than the overall median value of N_a are considered to be measurements made under high aerosol loading conditions. The mean value of N_a in the low and high aerosol loading categories is 255 and 714 cm^{-3}, respectively. Mean N_c increased by 29% from low to high aerosol conditions without changes in the mode value. Mean values of LWP and COD are slightly different, but their PDFs do not show any obvious difference under different aerosol loading conditions (Figs. 3b,c). Figure 3d shows that more samples with DER less than 8 μm are found when the aerosol loading is high and that more samples with DER greater than 12 μm are found when the aerosol loading is low. As the aerosol loading increases, the mean DER decreases by 8.1%. Figures 3a and 3d also show that high aerosol loading leads to a shift in the PDFs of N_c and DER toward larger and

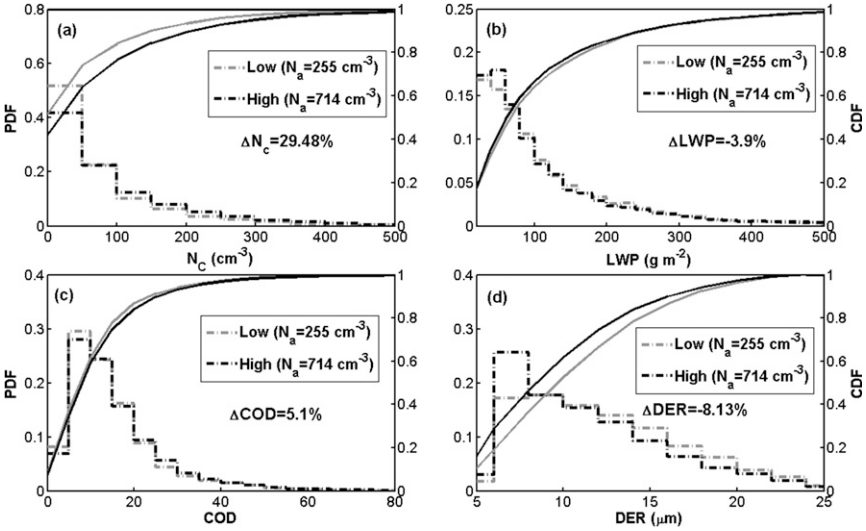

FIG. 3. PDFs (steps) and CDFs (curves) of (a) N_c, (b) LWP, (c) COD, and (d) DER under low (gray lines) and high (black lines) aerosol loading conditions. Numbers in each panel are the relative difference in each cloud property between high and low aerosol loading conditions.

smaller values, respectively, but does not result in a narrowing or broadening of their distributions. To unambiguously untangle the contributions of aerosol changes on cloud microphysical changes, investigations of aerosol–cloud interactions require that meteorological conditions remain the same. Figure 4 shows the means and standard deviations of meteorological variables under low and high aerosol loading conditions. The meteorological variables include temperature at 750 hPa, specific humidity at 750 hPa, relative humidity at 750 hPa, ω at 700 hPa, LTS, surface pressure, surface temperature, surface relative humidity, surface water vapor pressure, surface wind speed, and surface wind direction (from ''P1'' to ''P11'' in Fig. 4, respectively). There is no significant difference in any of the meteorological variables between low and high aerosol loading conditions, except for a weak difference in wind direction. The mean wind direction is 199° under low aerosol loading conditions and 169° under high aerosol loading conditions. The weak difference in wind direction under different aerosol conditions may indicate that different aerosol types dominated in each case (Logan et al. 2014).

c. *Influence of meteorological parameters on cloud properties and aerosol–cloud relationships*

1) INFLUENCE OF METEOROLOGICAL PARAMETERS ON CLOUD PROPERTIES

To illustrate the influence of meteorology on cloud properties, variations in cloud properties such as LTS and ω are shown in Fig. 5. To minimize the potential influence of aerosols, only samples with N_a less than 140 cm^{-3} are used, and the N_a stays constant with increasing LTS and ω. Figures 5a and 5b show that CBH and CTH significantly decrease as LTS increases. This is because strong stability confines the clouds to the boundary layer and inhibits the development and uplift of clouds, while extending their horizontal areal coverage (Matsui et al. 2004). Thus, more clouds with low

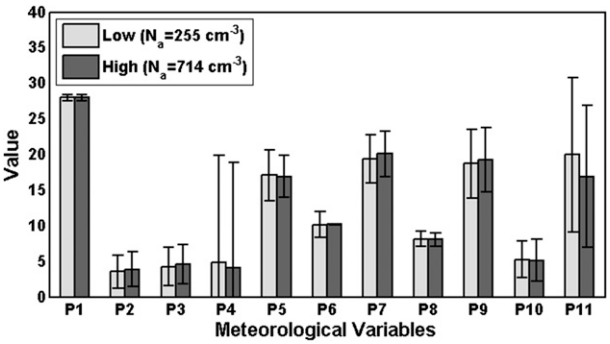

FIG. 4. Mean and std dev of selected meteorological variables under low (light gray bars) and high (dark gray bars) aerosol loading conditions. The meteorological variables are temperature at 750 hPa (T_{750}/10; K), specific humidity at 750 hPa [q(1000); g kg^{-1}], relative humidity at 750 hPa (RH_{750}/10; %), vertical velocity at 700 hPa [ω_{700}(100); Pa s^{-1}], lower-tropospheric stability (K), surface pressure (P_{sur}/100; hPa), surface temperature (°C), surface relative humidity (RH_{sur}/10; %), surface water vapor pressure (hPa), surface wind speed (m s^{-1}), and surface wind direction (WD_{sur}/10; °). These variables are identified by P1–P11, respectively.

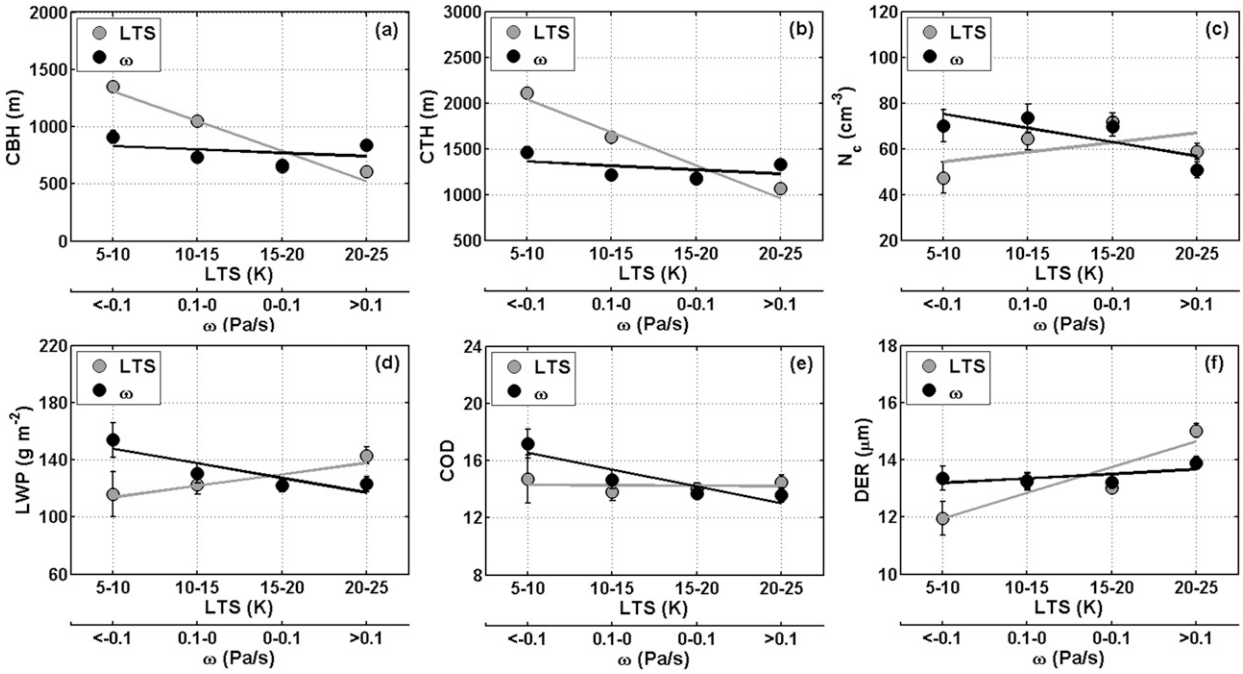

FIG. 5. (a) CBH, (b) CTH, (c) N_c, (d) LWP, (e) COD, and (f) DER as a function of LTS (gray dots and line) and ω (black dots and line).

CBH are observed under strong stability conditions. The CBH and CTH show a slight decrease with increasing ω (i.e., from ascending to descending motion), which is attributed to the inhibition of cloud development by descending motion. This illustrates that the CBH and CTH are more sensitive to thermodynamic conditions.

Figure 5c shows that N_c slightly increases as LTS increases. This is possible because moisture that has evaporated from the sea surface accumulates and gradually reaches saturation. More water vapor is supplied to the atmosphere, which decreases the competition for water vapor between CCN activation of aerosols, resulting in more CCN and cloud droplets when there is an inversion at the top of the boundary layer (Su et al. 2010; Dong et al. 2015). As ω increases, N_c decreases, which is consistent with results reported by others (e.g., Kim et al. 2008; Hudson and Noble 2014; West et al. 2014). This is because the stronger ascending motion enables more of the smaller aerosols to activate as a result of the increase in maximum supersaturation (West et al. 2014). The LWP is larger under more stable conditions (large LTS) than under less stable conditions and is larger for clouds with ascending motion than for clouds with descending motion (Fig. 5d). These results are consistent with those from studies using satellite measurements (e.g., Su et al. 2010), aircraft measurements (e.g., Cecchini et al. 2016), and model simulations (e.g., West et al. 2014). The COD is higher for clouds with ascending motion than for clouds with descending motion but remains constant as stability increases (Fig. 5e). In general, large values of LWP are associated with large values of COD. This correspondence can sometimes be inconsistent because of the nonlinear relationship between LWP and COD (Liu et al. 2013). Little change in COD as LTS increases likely happens because the observed trends in LWP and DER as LTS increases are similar. As LTS increases, DER increases, suggesting that DER is more sensitive to thermodynamic conditions than to the large-scale dynamic conditions seen in the cases considered here (Fig. 5f). These results are not consistent with results from some previous studies (e.g., Matsui et al. 2004; Lebsock et al. 2008) that reported DER decreases as stability increases because of the presence of a strong inversion inhibiting cloud droplet growth. An explanation for our results is that the LWP of clouds is enhanced under highly stable conditions, which supplies the water needed for cloud droplet growth (Su et al. 2010; Zhang et al. 2011). The increase in LWP is accompanied by an increase in droplet collision–coalescence, which is supported by the decrease in N_c with increasing LWP (see Fig. 8b, described in greater detail below, and the discussion in section 3d), leading to an increase in DER (Kim et al. 2008; McComiskey et al. 2009). A previous study showed that DER tends to be larger in ascending air than in descending air because clouds in a more convective regime ($\omega < 0$) tend to grow taller into the

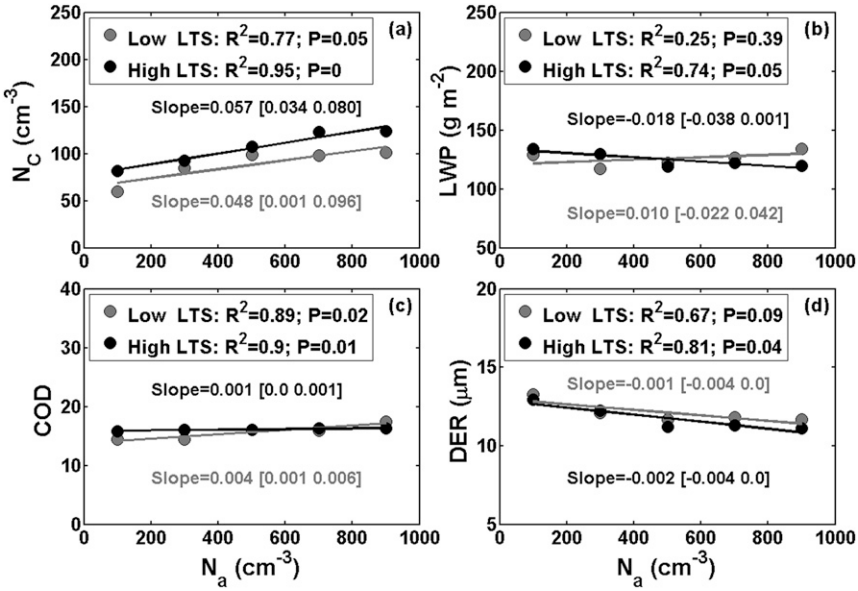

FIG. 6. (a) N_c, (b) LWP, (c) COD, and (d) DER as a function of N_a under low (gray lines) and high (black lines) atmospheric stability conditions. The slopes with their associated 95% confidence intervals under low (gray) and high (black) atmospheric stability conditions are given in each panel. The coefficient of determination R^2 and the statistical probability (P value) are shown.

atmosphere than do clouds in a subsidence regime ($\omega > 0$) (Su et al. 2010). However, this variation in DER is not observed in this study. It may be that greater N_c are found when $\omega < 0$ (West et al. 2014; Schmidt et al. 2015), resulting in a reduction in DER.

2) Response of cloud properties to aerosol loading according to meteorological conditions

Figure 6 shows how cloud properties change with increasing N_a under low and high stability conditions. The mean value of LTS for all selected samples was first calculated and is equal to 16.8 K. Samples under low and high stability conditions were then defined as those samples with LTS less than and greater than the overall mean value, respectively. The mean values of LTS for the low and high stability categories are 14.4 ± 2.1 and 18.6 ± 1.2 K, respectively. The cloud droplet number concentration significantly increases with increasing N_a in both LTS categories, suggesting no strong influence of stability on the relationship between N_c and N_a. The slope is stronger when atmospheric conditions are more stable (Fig. 6a). Large differences in the correlation between LWP and N_a exist between low and high atmospheric stability conditions. Under less stable conditions, LWP is constant with increasing N_a, but under more stable conditions a decrease in LWP with increasing N_a is seen. Clouds tend to have lower base heights under stable atmospheric conditions and so are more likely to interact and mix with aerosols, resulting in a stronger increase in N_c (Fig. 6a) and a decrease in LWP (Fig. 6b) (Jones et al. 2009; Costantino and Bréon 2013). COD increases as N_a increases under both stability conditions (Fig. 6c). The decrease in DER as N_a increases is more pronounced under more stable conditions than under less stable conditions because of the stronger increase in N_c with increasing N_a under more stable conditions. The decrease in LWP under more stable conditions could also contribute to the decrease in DER. This suggests that the response of cloud microphysical properties to aerosol loading is sensitive to atmospheric thermodynamic conditions. The implication is that an accurate quantification of AIE requires consideration of atmospheric thermodynamic conditions.

The influence of ω on the response of cloud properties to N_a is shown in Fig. 7. All samples are categorized into two ω ranges: $\omega < 0$ (ascending motion) and $\omega > 0$ (descending motion). The mean value of ω in each range is -0.096 and $0.104\,\mathrm{Pa\,s^{-1}}$, respectively. Overall, N_c shows a significant increase as N_a increases. The slope is larger when ascending-motion conditions are present (Fig. 7a), which is consistent with previous studies (e.g., Hudson and Noble 2014). This likely happens because the stronger ascending motion helps move more of the smaller aerosols to the upper parts of clouds

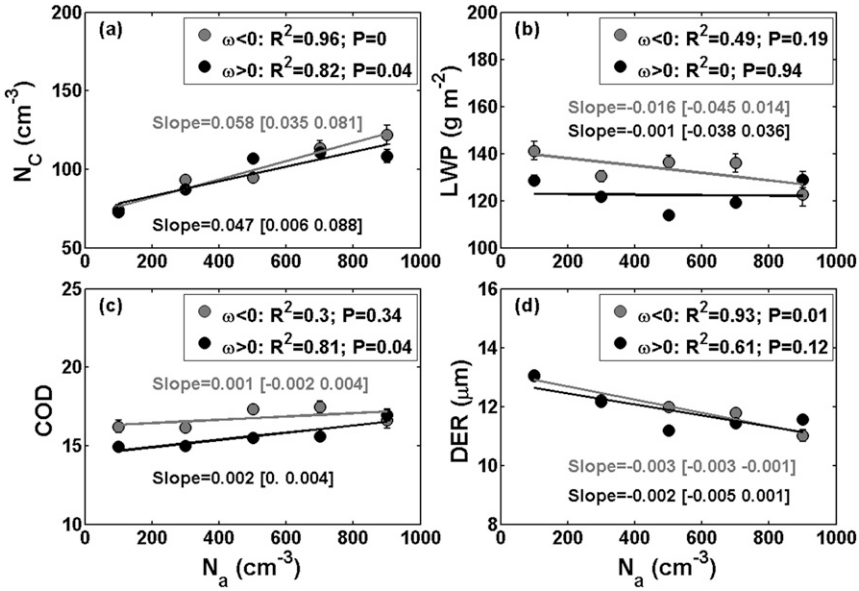

FIG. 7. As in Fig. 6, but for ascending- ($\omega < 0$; gray lines) and descending-motion ($\omega > 0$; black lines) conditions instead of atmospheric stability conditions. The slopes with their associated 95% confidence intervals for ascending- (gray) and descending-motion (black) conditions are given in each panel. The coefficient of determination R^2 and the statistical probability (P value) are shown.

and to activate as a result of the increase in supersaturation (Koike et al. 2012; West et al. 2014). The LWP is nearly constant under descending-motion conditions and decreases as N_a increases under ascending-motion conditions (Fig. 7b). There is a significant increase in COD as N_a increases under descending-motion conditions and a weaker increase under ascending-motion conditions (Fig. 7c). DER decreases with increasing N_a under both ascending- and descending-motion conditions (Fig. 7d), but the slope is stronger under ascending-motion conditions because of the stronger increase in N_c and the decrease in LWP.

d. *Quantifying the aerosol FIE*

The aerosol FIE is generally quantified as

$$\mathrm{FIE} = -\frac{\partial \ln(\mathrm{DER})}{\partial \ln(\alpha)},$$

where aerosol extinction α is a proxy for the CCN concentration. A constant LWP is assumed. It represents the relative change in mean cloud DER for a relative change in α for clouds having the same LWP (Feingold et al. 2003). Figure 8a shows DER as function of N_a for clouds with LWPs ranging from 100 to 120 g m^{-2}. The N_a bins range from 0 to 900 cm^{-3} in increments of 100 cm^{-3}, and the mean DER is calculated for each bin. The error bars represent the standard errors of the mean value, and the linear fit through the data points is represented by the solid gray line. The decrease in DER with increasing N_a is almost linear in log–log space. The magnitude of the FIE is 0.085 with an uncertainty of 0.022. Figure 8b shows the magnitude of the FIE in different LWP bins (filled circles, left ordinate). The black dots indicate values that are statistically significant at the 95% confidence level ($P = 0.05$). The LWP bins range from 20 to 240 g m^{-2} in increments of 20 g m^{-2}. The magnitude of the FIE, which is statistically significant at the 95% confidence level, ranges from 0.060 ± 0.022 to 0.101 ± 0.006 with a mean value of 0.074 ± 0.013. The magnitude of the FIE decreases as LWP increases, especially when LWP > 100 g m^{-2}. One explanation is that an increase in LWP is accompanied by an increase in droplet collision–coalescence, which masks the magnitude of the Twomey effect associated with drop activation (Kim et al. 2008; McComiskey et al. 2009). This is supported by the decrease in N_c with increasing LWP (Fig. 8b, gray triangles and line, right ordinate) because an increase in droplet collision–coalescence can partly lead to a reduction in N_c (McComiskey et al. 2009). Many studies have reported that the magnitude of the FIE generally lies between 0.02 and 0.33 (Rosenfeld and Feingold 2003; Feingold et al. 2006; McComiskey et al. 2009) and that most values of the FIE range from 0.05 to 0.25 (Zhao et al. 2012). The magnitude of the mean FIE found in this study falls within the range of reported values.

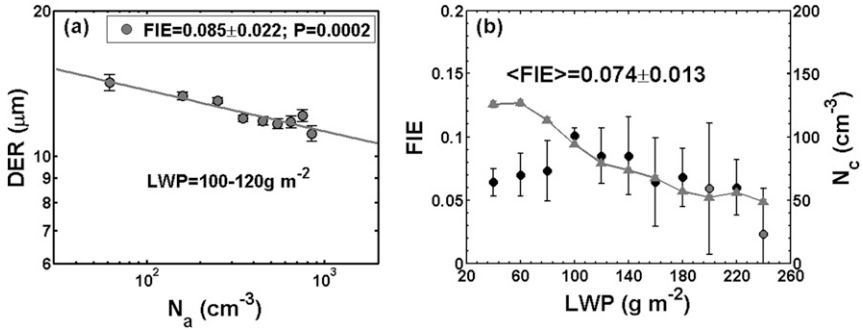

FIG. 8. (a) DER as a function of N_a for an example bin with a constant LWP of 100–120 g m^{-2} and (b) the quantified aerosol FIE with its uncertainty in each LWP bin (filled circles, left ordinate) and the changes in N_c with increasing LWP (gray triangles and line, right ordinate). The black dots indicate values that are statistically significant at the 95% confidence level (P = 0.05). The number is the mean value of FIE, which is statistically significant at the 95% confidence level for all LWP bins. Data collected under all meteorological conditions are used.

The magnitudes of the FIE with their uncertainties under different meteorological conditions were also examined and are shown in Fig. 9. Figure 9a shows DER as a function of N_a for cases where LWP ranges from 100 to 120 g m^{-2} and for low and high stability conditions. The magnitudes of the FIE and their uncertainties in each LWP bin and under low and high stability conditions are shown in Fig. 9b. The mean value of FIE is 0.059 ± 0.023 under less stable conditions and 0.088 ± 0.020 under more stable conditions. The differences in FIE under less and more stable conditions are statistically significant at the 95% confidence level. These results show that the FIE tends to be larger under more stable conditions. This suggests that, when the atmospheric environment becomes more stable, the relative susceptibility of cloud DER to aerosols becomes stronger. Studies using aerosol and marine warm cloud properties from MODIS retrievals over the west coast of Africa (Su et al. 2010), the East China Sea (Wang et al. 2014), and the global ocean between 60°S and 60°N (Chen et al. 2014) showed opposite results: namely, that DER is more sensitive to aerosol changes under less stable conditions than under more stable conditions. Under unstable conditions, more aerosols can reach cloud tops and interact with cloud droplets. Because DER retrievals from MODIS are typically representative of cloud particle sizes near the top of optically thick clouds (Chang and Li 2002, 2003), satellite-retrieved DER is more affected (Su et al. 2010). Radar-retrieved DER data represent layer-mean particle sizes. Based on five years of *Cloud–Aerosol Lidar and Infrared Pathfinder Satellite Observations* measurements, Huang et al. (2013) showed that aerosol extinction coefficients decreased from the surface to high altitudes and that most aerosol particles were located in the boundary layer over the North Atlantic region. Under more stable atmospheric conditions, CBHs are generally lower than those under less stable conditions (e.g., Fig. 5a) and thus can mix and interact more with aerosols, resulting in a larger FIE (Jones et al. 2009; Costantino and Bréon 2013). This is confirmed by the relationship between DER and N_a under constant LWP conditions for samples with low and high CBHs (Fig. 10). The FIE is generally larger for clouds with low CBHs than for clouds with high CBHs. The differences are statistically significant at the 95% confidence level. Samples with low and high CBHs are defined as those samples with CBHs less than and greater than the overall mean CBH of all samples, respectively. This result implies that the dependence of the response of cloud properties to aerosol perturbations on thermodynamic conditions appears to vary according to the approach used to retrieve cloud properties.

To test this hypothesis, the FIE was also calculated using matched data from *Terra*/MODIS and *Aqua*/MODIS cloud products and surface-measured N_a from the study site during the campaign period. The MODIS level-2 product (MOD06 and MYD06) provides cloud optical and microphysical properties at a 1-km resolution. Retrievals from pixels falling within 5 km of the study site were selected. Only nonprecipitating and single-layer liquid water cloud retrievals were considered. Surface-measured N_a averaged within a 1-h time interval centered on the time of a MODIS overpass was used. Figure 11a shows DER as a function of N_a for cases where LWP ranges from 60 to 90 g m^{-2} under low and high stability conditions. The magnitudes of the FIE with their uncertainties in four LWP bins under low and high stability conditions are given in Fig. 11b. The number above each bar in Fig. 11b is the number of samples used in the calculation. The largest FIE occurs

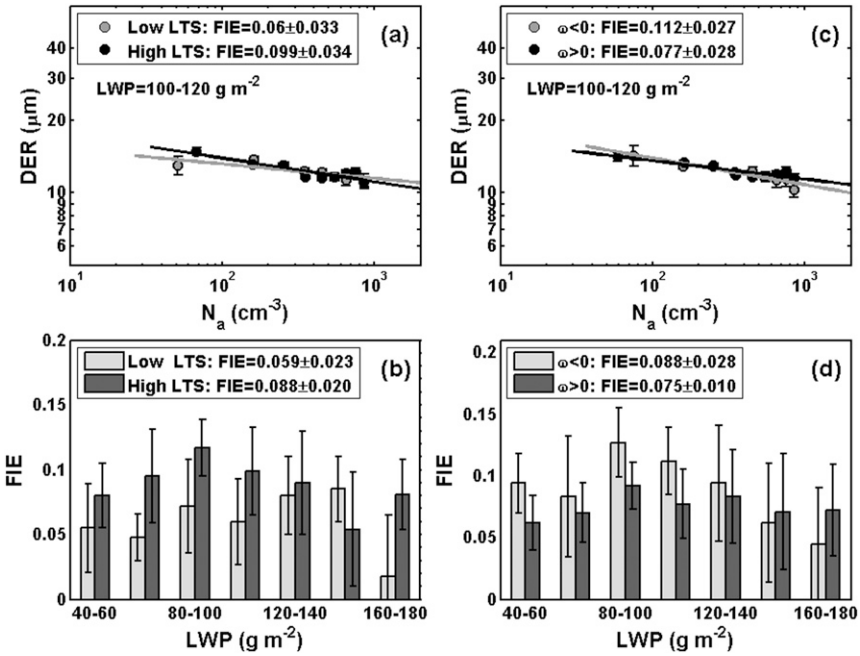

FIG. 9. (a) DER as a function of N_a for an example bin with a constant LWP of 100–120 g m^{-2} under less (gray) and more (black) stable atmospheric conditions; (b) the magnitude and corresponding uncertainty of the aerosol FIE in each LWP bin under less (light gray bars) and more (dark gray bars) stable atmospheric conditions; (c) as in (a), but for ascending- (gray) and descending-motion (black) cases; (d) as in (b), but for ascending- (light gray bars) and descending-motion (dark gray bars) cases. Mean values of the FIE under different conditions are shown in (a)–(d).

under less stable conditions across all LWP bins. The differences are statistically significant at the 95% confidence level. Long-term (2000–14) *Terra*/MODIS level-3 (MOD08) aerosol and cloud products associated with ECMWF Re-Analysis data from the 1° × 1° grid box closest to the field campaign site are used to repeat calculations of the FIE and their uncertainties under low and high stable conditions. Although level-3 AOD retrievals have less cloud contamination (Niu and Li 2012), further measures were taken to reduce the possibility of cloud contamination in the AOD retrieval: namely, excluding grid boxes with AOD > 0.6. As before, only nonprecipitating and single-layer liquid water cloud retrievals were considered. Figure 12a shows that

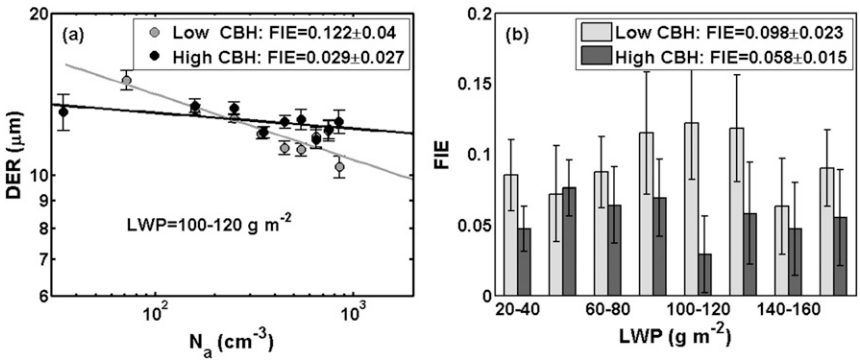

FIG. 10. (a) DER as a function of N_a for an example bin with a constant LWP of 100–120 g m^{-2} and for clouds with low (gray points and line) and high cloud-base heights (black points and line); (b) the magnitude and corresponding uncertainty of the aerosol FIE in each LWP bin for clouds with low (light gray bars) and high cloud-base heights (dark gray bars). Mean values of the FIE under different conditions are shown.

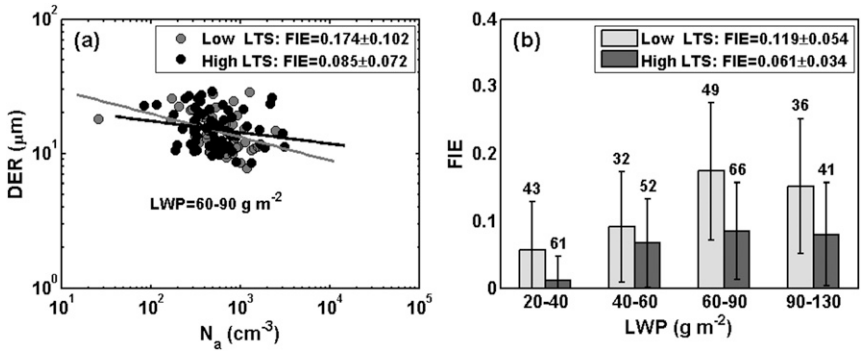

FIG. 11. (a) DER as a function of N_a for an example bin with a constant LWP of 60–90 g m^{-2} under less (gray) and more (black) atmospherically stable conditions; (b) the magnitude and corresponding uncertainty of the aerosol FIE in each LWP bin under less (light gray bars) and more (dark gray bars) atmospherically stable conditions. Numbers above each bar in (b) are the number of samples that went into the calculation of the FIE. LWP and DER are from *Terra*/MODIS and *Aqua*/MODIS retrievals from pixels falling within 5 km of the site during the field campaign.

the FIE is generally larger under less stable conditions across almost all LWP bins. The differences are statistically significant at the 95% confidence level. The results from Figs. 11b and 12a confirm the hypothesis put forward earlier on: that is, the dependence of the response of cloud properties to aerosol perturbations on thermodynamic conditions appears to vary according to the approach used to retrieve cloud properties.

Figures 9c and 9d show the magnitudes of FIE and their uncertainties for cases where LWP ranges from 100 to 120 g m^{-2} and for all LWP bins under ascending- ($\omega < 0$) and descending-motion ($\omega > 0$) conditions. Overall, the mean value of FIE for all LWP cases under ascending-motion conditions is larger than that under descending-motion conditions because of the increase in N_c with increasing ascending motion, which is in accord with some previous studies (e.g., McComiskey et al. 2009; West et al. 2014). The FIE varies more as LWP changes under ascending-motion conditions than under descending-motion conditions. The magnitude of the FIE tends to be higher under ascending-motion conditions for clouds with low LWP values and higher under descending-motion conditions for clouds with high LWP values. This is also seen in Fig. 12b.

4. Conclusions

Macro- and microphysical properties of aerosols and marine boundary layer clouds at a site in the Azores were analyzed using a 19-month dataset compiled during the Clouds, Aerosol, and Precipitation in the Marine Boundary Layer field campaign to examine which

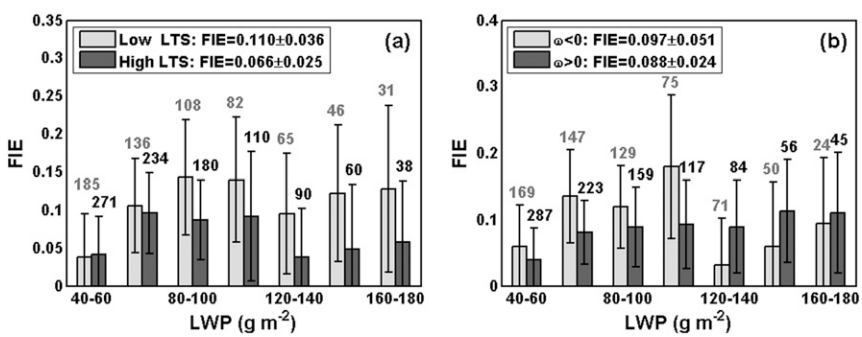

FIG. 12. Magnitude and corresponding uncertainty of the aerosol FIE in each LWP bin under (a) low (light gray bars) and high (dark gray bars) LTS conditions and under (b) ascending- (light gray bars) and descending-motion (dark gray bars) conditions. The gray (black) numbers indicate the number of samples that went into the calculation of the FIE. Aerosol and cloud data are from the *Terra*/MODIS level-3 product, and meteorological variables are from ECMWF Re-Analysis data from 2000 to 2014 in the 1° × 1° grid box closest to the site.

processes control the diversity in the sensitivity of low clouds to aerosol perturbations. This is one of the most important science questions in the study of cloud–aerosol–precipitation interactions. The influence of large-scale dynamic and thermodynamic effects was taken into account. This was achieved by constraining aerosol–cloud data pairs to a narrow range of meteorological parameters so that the contribution of large-scale circulation to the diversity in the sensitivity of warm low clouds to aerosol perturbations could be examined.

Variations in cloud properties as aerosol loading increases were first examined. There is a slight decrease in LWP with increasing N_a. This is because the inhibited cloud droplet sedimentation due to the reduced cloud droplet size likely enhances evaporation and entrainment at the cloud top, resulting in a reduction in the LWPs of nonprecipitating clouds. As N_a increases, N_c and COD increase significantly, but DER decreases noticeably. This suggests that aerosols enhance the cloud number concentration and inhibit the growth of cloud droplets. The effect of meteorological parameters on cloud properties is examined by constraining aerosols to a low concentration and by keeping the concentration constant as meteorological conditions change. Both CBH and CTH show a significant decrease with increasing atmospheric stability and a slight increase when transitioning from ascending- to descending-motion conditions. As atmospheric stability increases, N_c, LWP, and DER also increase, but COD remains constant. Clear decreasing trends in N_c, LWP, and COD are seen when the cloud vertical motion changes from ascending to descending. However, the DER remains constant for all values of ω.

Cloud droplet number concentration and COD significantly increase with increasing N_a under both low and high stable conditions. The relationships are stronger when atmospheric conditions are stable. Under less stable conditions, LWP is constant as N_a increases, but under more stable conditions, a significant decrease in LWP as N_a increases is seen. The negative relationship between DER and N_a is stronger under more stable conditions than under less stable conditions. This is because clouds tend to have lower base heights under stable atmospheric conditions and so are more likely to interact and mix with aerosols, resulting in a stronger increase in N_c and a decrease in LWP and DER. Under both ascending- and descending-motion conditions, N_c shows a significant increase as N_a increases. A larger slope is found under ascending-motion conditions than under descending-motion conditions. The LWP is nearly constant as N_a increases under descending-motion conditions and slightly decreases under ascending-motion conditions. The COD (DER) increases (decreases) with increasing N_a under both ascending- and descending-motion conditions, but the trend in COD (DER) is stronger under descending (ascending)-motion conditions. The stronger relationship between N_c (LWP and DER) and N_a under ascending conditions is partly because the higher ascending motion enables more of the smaller aerosols to move to the upper parts of clouds and to activate as a result of the increase in supersaturation.

By constraining LWP to a fixed range of values, the FIE is quantified by analyzing the relative susceptibility of DER to N_a. The magnitude and corresponding uncertainty of the FIE ranges from 0.060 ± 0.022 to 0.101 ± 0.006 in different LWP bins with a clear decreasing trend as LWP increases. Greater differences in the magnitude of the FIE are observed depending on atmospheric stability and vertical motion conditions. The magnitudes of FIE, calculated from surface-retrieved cloud properties, are larger under more atmospherically stable conditions, while the magnitudes of FIE calculated from satellite-retrieved cloud properties show an opposite relationship. This happens because the satellite can only detect cloud droplet effective radii near cloud tops. The magnitude of the FIE changes more under ascending-motion conditions as LWP changes. It appears to be higher under ascending-motion conditions for clouds with low LWP and under descending-motion conditions for clouds with high LWP. The contrasting dependence of FIE on atmospheric stability estimated from surface- and satellite-retrieved cloud properties implies that the dependence of the response of cloud properties to aerosol perturbations on thermodynamic conditions appears to vary according to the approach used to retrieve cloud properties. This underscores the importance of assessing all-level properties of clouds in aerosol–cloud interaction studies.

Acknowledgments. The ground-based measurements were obtained from the Atmospheric Radiation Measurement (ARM) program sponsored by the U.S. Department of Energy (DOE) Office of Energy Research, Office of Health and Environmental Research, Environmental Sciences Division. Cloud property retrieval products for Graciosa Island, Azores, are from the ARM principal investigator (PI) product developed by Dr. Xiquan Dong at the University of North Dakota. The large-scale dynamic and thermodynamic data are obtained from the European Centre for Medium-Range Weather Forecasts (ECMWF) model runs for ARM analysis provided by the ECMWF. The study is supported by the following research grants: MOST (2013CB955804), NSFC (91544217), NSF (AGS1534670), NOAA (NA15NWS4680011), and DOE (DES0007171).

REFERENCES

Albrecht, B. A., 1989: Aerosols, cloud microphysics, and fractional cloudiness. *Science*, **245**, 1227–1230, doi:10.1126/science.245.4923.1227.

Bony, S., and J. L. Dufresne, 2005: Marine boundary layer clouds at the heart of cloud feedback uncertainties in climate models. *Geophys. Res. Lett.*, **32**, L20806, doi:10.1029/2005GL023851.

——, ——, H. Le Treut, J. J. Morcrette, and C. Senior, 2004: On dynamic and thermodynamic components of cloud changes. *Climate Dyn.*, **22**, 71–86, doi:10.1007/s00382-003-0369-6.

Bretherton, C. S., P. N. Blossery, and J. Uchida, 2007: Cloud droplet sedimentation, entrainment efficiency, and subtropical stratocumulus albedo. *Geophys. Res. Lett.*, **34**, L03813, doi:10.1029/2006GL027648.

Cecchini, M. A., and Coauthors, 2016: Impacts of the Manaus pollution plume on the microphysical properties of Amazonian warm-phase clouds in the wet season. *Atmos. Chem. Phys.*, **16**, 7029–7041, doi:10.5194/acp-16-7029-2016.

Chang, F.-L., and Z. Li, 2002: Estimating the vertical variation of cloud droplet effective radius using multispectral near-infrared satellite measurements. *J. Geophys. Res.*, **107**, AAC 7-1–AAC 7-2, doi:10.1029/2001JD000766.

——, and ——, 2003: Retrieving vertical profiles of water-cloud droplet effective radius: Algorithm modification and preliminary application. *J. Geophys. Res.*, **108**, 4763, doi:10.1029/2003JD003906.

Chen, Y.-C., M. W. Christensen, G. L. Stephens, and J. H. Seinfeld, 2014: Satellite-based estimate of global aerosol–cloud radiative forcing by marine warm clouds. *Nat. Geosci.*, **7**, 643–646, doi:10.1038/ngeo2214.

Clothiaux, E. E., T. P. Ackerman, G. G. Mace, K. P. Moran, R. T. Marchand, M. A. Miller, and B. E. Martner, 2000: Objective determination of cloud heights and radar reflectivities using a combination of active remote sensors at the ARM CART sites. *J. Appl. Meteor.*, **39**, 645–665, doi:10.1175/1520-0450(2000)039<0645:ODOCHA>2.0.CO;2.

Costantino, L., and F. M. Bréon, 2013: Aerosol indirect effect on warm clouds over South-East Atlantic, from co-located MODIS and *CALIPSO* observations. *Atmos. Chem. Phys.*, **13**, 69–88, doi:10.5194/acp-13-69-2013.

Dong, X., and G. G. Mace, 2003: Profiles of low-level stratus cloud microphysics deduced from ground-based measurements. *J. Atmos. Oceanic Technol.*, **20**, 42–53, doi:10.1175/1520-0426(2003)020<0042:POLLSC>2.0.CO;2.

——, T. P. Ackerman, E. E. Clothiaux, P. Pilewskie, and Y. Han, 1997: Microphysical and radiative properties of stratiform clouds deduced from ground-based measurements. *J. Geophys. Res.*, **102**, 23 829–23 843, doi:10.1029/97JD02119.

——, ——, and ——, 1998: Parameterizations of microphysical and shortwave radiative properties of boundary layer stratus from ground-based measurements. *J. Geophys. Res.*, **103**, 31 681–31 693, doi:10.1029/1998JD200047.

——, P. Minnis, T. P. Ackerman, E. E. Clothiaux, G. G. Mace, C. N. Long, and J. C. Liljegren, 2000: A 25-month database of stratus cloud properties generated from ground-based measurements at the Atmospheric Radiation Measurement Southern Great Plains site. *J. Geophys. Res.*, **105**, 4529–4538, doi:10.1029/1999JD901159.

——, ——, B. Xi, S. Sun-Mack, and Y. Chen, 2008: Comparison of CERES-MODIS stratus cloud properties with ground-based measurements at the DOE ARM Southern Great Plains site. *J. Geophys. Res.*, **113**, D03204, doi:10.1029/2007JD008438.

——, B. Xi, A. Kennedy, P. Minnis, and R. Wood, 2014a: A 19-month record of marine aerosol–cloud–radiation properties derived from DOE ARM Mobile Facility deployment at the Azores. Part I: Cloud fraction and single-layered MBL cloud properties. *J. Climate*, **27**, 3665–3682, doi:10.1175/JCLI-D-13-00553.1.

——, ——, and P. Wu, 2014b: Investigation of the diurnal variation of marine boundary layer cloud microphysical properties at the Azores. *J. Climate*, **27**, 8827–8835, doi:10.1175/JCLI-D-14-00434.1.

——, A. C. Schwants, B. Xi, and P. Wu, 2015: Investigation of the marine boundary layer cloud properties under coupled and decoupled conditions over the Azores. *J. Geophys. Res. Atmos.*, **120**, 6179–6191, doi:10.1002/2014JD022939.

ECMWF, 1994: The description of the ECMWF/WCRP Level III—A global atmospheric data archive. ECMWF Tech. Rep., 48 pp. [Available online at http://cedadocs.badc.rl.ac.uk/1109/.]

Feingold, G., L. A. Remer, J. Ramaprasad, and Y. J. Kaufman, 2001: Analysis of smoke impact on clouds in Brazilian biomass burning regions: An extension of Twomey's approach. *J. Geophys. Res.*, **106**, 22 907–22 922, doi:10.1029/2001JD000732.

——, W. L. Eberhard, D. E. Veron, and M. Previdi, 2003: First measurements of the Twomey indirect effect using ground-based remote sensors. *Geophys. Res. Lett.*, **30**, 1287, doi:10.1029/2002GL016633.

——, R. Furrer, P. Pilewskie, L. A. Remer, Q. Min, and H. Jonsson, 2006: Aerosol indirect effect studies at Southern Great Plains during the May 2003 Intensive Operations Period. *J. Geophys. Res.*, **111**, D05S14, doi:10.1029/2004JD005648.

Hill, A. A., and G. Feingold, 2009: The influence of entrainment and mixing assumption on aerosol–cloud interactions in marine stratocumulus. *J. Atmos. Sci.*, **66**, 1450–1464, doi:10.1175/2008JAS2909.1.

Huang, L., J. H. Jiang, J. L. Tackett, H. Su, and R. Fu, 2013: Seasonal and diurnal variations of aerosol extinction profile and type distribution from *CALIPSO* 5-year observations. *J. Geophys. Res. Atmos.*, **118**, 4572–4596, doi:10.1002/jgrd.50407.

Hudson, J. G., and S. Noble, 2014: CCN and vertical velocity influences on droplet concentrations and supersaturations in clean and polluted stratus clouds. *J. Atmos. Sci.*, **71**, 312–331, doi:10.1175/JAS-D-13-086.1.

IPCC, 2013: *Climate Change 2013: The Physical Science Basis*. Cambridge University Press, 1535 pp., doi:10.1017/CBO9781107415324.

Jefferson, A., 2011: Aerosol Observing System (AOS) handbook. U.S. DOE Office of Science Tech. Rep. ARM-TR-014, 32 pp. [Available online at https://www.arm.gov/publications/tech_reports/handbooks/aos_handbook.pdf.]

Jeong, M. J., and Z. Li, 2010: Separating real and apparent effects of cloud, humidity, and dynamics on aerosol optical thickness near cloud edges. *J. Geophys. Res.*, **115**, D00K32, doi:10.1029/2009JD013547.

Jones, T. A., S. A. Christopher, and J. Quaas, 2009: A six year satellite-based assessment of the regional variations in aerosol indirect effects. *Atmos. Chem. Phys.*, **9**, 4091–4114, doi:10.5194/acp-9-4091-2009.

Kaufman, Y. J., I. K. Lorraine, A. Remer, D. Rosenfeld, and Y. Rudich, 2005: The effect of smoke, dust, and pollution aerosol on shallow cloud development over the Atlantic Ocean. *Proc. Natl. Acad. Sci. USA*, **102**, 11 207–11 212, doi:10.1073/pnas.0505191102.

Kim, B.-G., M. A. Miller, S. E. Schwartz, Y. Liu, and Q. Min, 2008: The role of adiabaticity in the aerosol first indirect effect. *J. Geophys. Res.*, **113**, D05210, doi:10.1029/2007JD008961.

Koike, M., and Coauthors, 2012: Measurements of regional-scale aerosol impacts on cloud microphysics over the East China Sea: Possible influences of warm sea surface temperature over the Kuroshio ocean current. *J. Geophys. Res.*, **117**, D17205, doi:10.1029/2011JD017324.

Koren, I., G. Feingold, and L. A. Remer, 2010: The invigoration of deep convective clouds over the Atlantic: Aerosol effect, meteorology or retrieval artifact? *Atmos. Chem. Phys.*, **10**, 8855–8872, doi:10.5194/acp-10-8855-2010.

Lebsock, M. D., G. L. Stephens, and C. Kummerow, 2008: Multisensor satellite observations of aerosol effects on warm clouds. *J. Geophys. Res.*, **113**, D15205, doi:10.1029/2008JD009876.

Lee, S. S., J. E. Penner, and S. M. Saleeby, 2009: Aerosol effects on liquid-water path of thin stratocumulus clouds. *J. Geophys. Res.*, **114**, D07204, doi:10.1029/2008JD010513.

Leith, C. E., 1973: The standard error of time-average estimates of climatic means. *J. Appl. Meteor.*, **12**, 1066–1069, doi:10.1175/1520-0450(1973)012<1066:TSEOTA>2.0.CO;2.

Li, Z., and Coauthors, 2009: Uncertainties in satellite remote sensing of aerosols and impact on monitoring its long-term trend: A review and perspective. *Ann. Geophys.*, **27**, 2755–2770, doi:10.5194/angeo-27-2755-2009.

——, F. Niu, J. Fan, Y. Liu, D. Rosenfeld, and Y. Ding, 2011: Long-term impacts of aerosols on the vertical development of clouds and precipitation. *Nat. Geosci.*, **4**, 888–894, doi:10.1038/ngeo1313.

Liljegren, J. C., E. E. Clothiaux, G. G. Mace, S. Kato, and X. Dong, 2001: A new retrieval for cloud liquid water path using a ground-based microwave radiometer and measurements of cloud temperature. *J. Geophys. Res.*, **106**, 14 485–14 500, doi:10.1029/2000JD900817.

Liu, J., and Z. Li, 2014: Estimation of cloud condensation nuclei concentration from aerosol optical quantities: Influential factors and uncertainties. *Atmos. Chem. Phys.*, **14**, 471–483, doi:10.5194/acp-14-471-2014.

——, Y. Zheng, Z. Li, and M. Cribb, 2011: Analysis of cloud condensation nuclei properties at a polluted site in southeastern China during the AMF-China Campaign. *J. Geophys. Res.*, **116**, D00K35, doi:10.1029/2011JD016395.

——, ——, ——, C. Flynn, and M. Cribb, 2012: Seasonal variations of aerosol optical properties, vertical distribution and associated radiative effects in the Yangtze Delta region of China. *J. Geophys. Res.*, **117**, D00K38, doi:10.1029/2011JD016490.

——, Z. Li, Y. Zheng, J. C. Chiu, F. Zhao, M. Cadeddu, F. Weng, and M. Cribb, 2013: Cloud optical and microphysical properties derived from ground-based and satellite sensors over a site in the Yangtze Delta region. *J. Geophys. Res. Atmos.*, **118**, 9141–9152, doi:10.1002/jgrd.50648.

Logan, T., B. Xi, and X. Dong, 2014: Aerosol properties and their influences on marine boundary layer cloud condensation nuclei at the ARM Mobile Facility over the Azores. *J. Geophys. Res. Atmos.*, **119**, 4859–4872, doi:10.1002/2013JD021288.

Mather, J. H., and J. W. Voyles, 2013: The ARM Climate Research Facility: A review of structure and capabilities. *Bull. Amer. Meteor. Soc.*, **94**, 377–392, doi:10.1175/BAMS-D-11-00218.1.

Matsui, T., H. Masunaga, R. A. S. Pielke, and W. K. Tao, 2004: Impact of aerosols and atmospheric thermodynamics on cloud properties within the climate system. *Geophys. Res. Lett.*, **31**, L06109, doi:10.1029/2003GL019287.

McComiskey, A., G. Feingold, A. S. Frisch, D. D. Turner, M. A. Miller, J. C. Chiu, Q. Min, and J. A. Ogren, 2009: An assessment of aerosol–cloud interactions in marine stratus clouds based on surface remote sensing. *J. Geophys. Res.*, **114**, D09203, doi:10.1029/2008JD011006.

Medeiros, B., and B. Stevens, 2011: Revealing differences in GCM representations of low clouds. *Climate Dyn.*, **36**, 385–399, doi:10.1007/s00382-009-0694-5.

Menon, S., A. D. Del Genio, Y. Kaufman, R. Bennartz, D. Koch, N. Loeb, and D. Orlikowski, 2008: Analyzing signatures of aerosol–cloud interactions from satellite retrievals and the GISS GCM to constrain the aerosol indirect effect. *J. Geophys. Res.*, **113**, D14S22, doi:10.1029/2007JD009442.

Miles, N. L., J. Verlinde, and E. E. Clothiaux, 2000: Cloud-droplet size distributions in low-level stratiform clouds. *J. Atmos. Sci.*, **57**, 295–311, doi:10.1175/1520-0469(2000)057<0295:CDSDIL>2.0.CO;2.

Nakajima, T., A. Higurashi, K. Kawamoto, and J. E. Penner, 2001: A possible correlation between satellite-derived cloud and aerosol microphysical parameters. *Geophys. Res. Lett.*, **28**, 1171–1174, doi:10.1029/2000GL012186.

Niu, F., and Z. Li, 2012: Systematic variations of cloud top temperature and precipitation rate with aerosols over the global tropics. *Atmos. Chem. Phys.*, **12**, 8491–8498, doi:10.5194/acp-12-8491-2012.

Painemal, D., and P. Zuidema, 2013: The first aerosol indirect effect quantified through airborne remote sensing during VOCALS-Rex. *Atmos. Chem. Phys.*, **13**, 917–931, doi:10.5194/acp-13-917-2013.

Pandithurai, G., T. Takamura, J. Yamaguchi, K. Miyagi, T. Takano, Y. Ishizaka, S. Dipu, and A. Shimizu, 2009: Aerosol effect on cloud droplet size as monitored from surface-based remote sensing over East China Sea region. *Geophys. Res. Lett.*, **36**, L13805, doi:10.1029/2009GL038451.

Quaas, J., and Coauthors, 2009: Aerosol indirect effects—General circulation model intercomparison and evaluation with satellite data. *Atmos. Chem. Phys.*, **9**, 8697–8717, doi:10.5194/acp-9-8697-2009.

Rosenfeld, D., and G. Feingold, 2003: Explanation of the discrepancies among satellite observations of the aerosol indirect effects. *Geophys. Res. Lett.*, **30**, 1776, doi:10.1029/2003GL017684.

Schmidt, J., A. Ansmann, J. Buhl, and U. Wandinger, 2015: A strong aerosol–cloud interaction in altocumulus during updraft periods: Lidar observations over central Europe. *Atmos. Chem. Phys.*, **15**, 10 687–10 700, doi:10.5194/acp-15-10687-2015.

Su, W., N. G. Loeb, K. M. Xu, G. L. Schuster, and Z. A. Eitzen, 2010: An estimate of aerosol indirect effect from satellite measurements with concurrent meteorological analysis. *J. Geophys. Res.*, **115**, D18219, doi:10.1029/2010JD013948.

Teller, A., and Z. Levin, 2006: The effects of aerosols on precipitation and dimensions of subtropical clouds: A sensitivity study using a numerical cloud model. *Atmos. Chem. Phys.*, **6**, 67–80, doi:10.5194/acp-6-67-2006.

Twohy, C. H., M. D. Petters, J. R. Snider, B. Stevens, W. Tahnk, M. Wetzel, L. Russell, and F. Burnet, 2005: Evaluation of the aerosol indirect effect in marine stratocumulus clouds: Droplet number, size, liquid water path, and radiative impact. *J. Geophys. Res.*, **110**, D08203, doi:10.1029/2004JD005116.

——, and Coauthors, 2013: Impacts of aerosol particles on the microphysical and radiative properties of stratocumulus clouds over the southeast Pacific Ocean. *Atmos. Chem. Phys.*, **13**, 2541–2562, doi:10.5194/acp-13-2541-2013.

Twomey, S., 1977: The influence of pollution on the shortwave albedo of clouds. *J. Atmos. Sci.*, **34**, 1149–1152, doi:10.1175/1520-0469(1977)034<1149:TIOPOT>2.0.CO;2.

Várnai, T., and A. Marshak, 2014: Near-cloud aerosol properties from the 1 km resolution MODIS ocean product. *J. Geophys. Res. Atmos.*, **119**, 1546–1554, doi:10.1002/2013JD020633.

Wang, F., J. Guo, Y. Wu, X. Zheng, M. Deng, X. Li, J. Zhang, and J. Zhao, 2014: Satellite observed aerosol-induced variability in warm cloud properties under different meteorological conditions over eastern China. *Atmos. Environ.*, **84**, 122–132, doi:10.1016/j.atmosenv.2013.11.018.

Wang, Y., J. Fan, R. Zhang, L. R. Leung, and C. Franklin, 2013: Improving bulk microphysics parameterizations in simulations of aerosol effects. *J. Geophys. Res. Atmos.*, **118**, 5361–5379, doi:10.1002/jgrd.50432.

Wang, Z., and K. Sassen, 2001: Cloud type and macrophysical property retrieval using multiple remote sensors. *J. Appl. Meteor.*, **40**, 1665–1682, doi:10.1175/1520-0450(2001)040<1665:CTAMPR>2.0.CO;2.

West, R. E. L., P. Stier, A. Jones, C. E. Johnson, G. W. Mann, N. Bellouin, D. G. Partridge, and Z. Kipling, 2014: The importance of vertical velocity variability for estimates of the indirect aerosol effects. *Atmos. Chem. Phys.*, **14**, 6369–6393, doi:10.5194/acp-14-6369-2014.

Wood, R., 2009: Clouds, Aerosol, and Precipitation in the Marine Boundary Layer (CAP-MBL). U.S. DOE Office of Science Tech. Rep. DOE/SC-ARM-0902, 29 pp. [Available online at http://www.arm.gov/publications/programdocs/doe-sc-arm-0902.pdf?id=71.]

——, and C. S. Bretherton, 2006: On the relationship between stratiform low cloud cover and lower-tropospheric stability. *J. Climate*, **19**, 6425–6432, doi:10.1175/JCLI3988.1.

——, and Coauthors, 2015: Clouds, Aerosols, and Precipitation in the Marine Boundary Layer: An ARM Mobile Facility deployment. *Bull. Amer. Meteor. Soc.*, **96**, 419–440, doi:10.1175/BAMS-D-13-00180.1.

Xi, B., X. Dong, P. Minnis, and S. Sun-Mack, 2014: Comparison of marine boundary layer cloud properties from CERES-MODIS edition 4 and DOE ARM AMF measurements at the Azores. *J. Geophys. Res. Atmos.*, **119**, 9509–9529, doi:10.1002/2014JD021813.

Zhang, Q., J. Quan, X. Tie, M. Huang, and X. Ma, 2011: Impact of aerosol particles on cloud formation: Aircraft measurements in China. *Atmos. Environ.*, **45**, 665–672, doi:10.1016/j.atmosenv.2010.10.025.

Zhao, C., S. A. Klein, S. Xie, X. Liu, J. S. Boyle, and Y. Zhang, 2012: Aerosol first indirect effects on non-precipitating low-level liquid cloud properties as simulated by CAM5 at ARM sites. *Geophys. Res. Lett.*, **39**, L08806, doi:10.1029/2012GL051213.

Zheng, X., B. Albrecht, P. Minnis, K. Ayers, and H. H. Jonson, 2010: Observed aerosol and liquid water path relationships in marine stratocumulus. *Geophys. Res. Lett.*, **37**, L17803, doi:10.1029/2010GL044095.